Controlling product selectivity in hybrid gas/liquid reactors using gas conditions, voltage, and temperature

Seung-Hoon Lee,¹ Brandon Iglesias,² Henry O. Everitt,^{3,4,*} and Jie Liu^{1,*}

¹Department of Chemistry, Duke University, Durham, North Carolina 27708, USA

²Reactwell, L.L.C. 6501 Navigation Blvd, Houston, TX 77011, USA

³U.S. Army DEVCOM Army Research Laboratory-South/Rice University, 6100 Main St.,

Houston, TX 77005 USA

⁴Department of Physics, Duke University, Durham, North Carolina 27708, USA

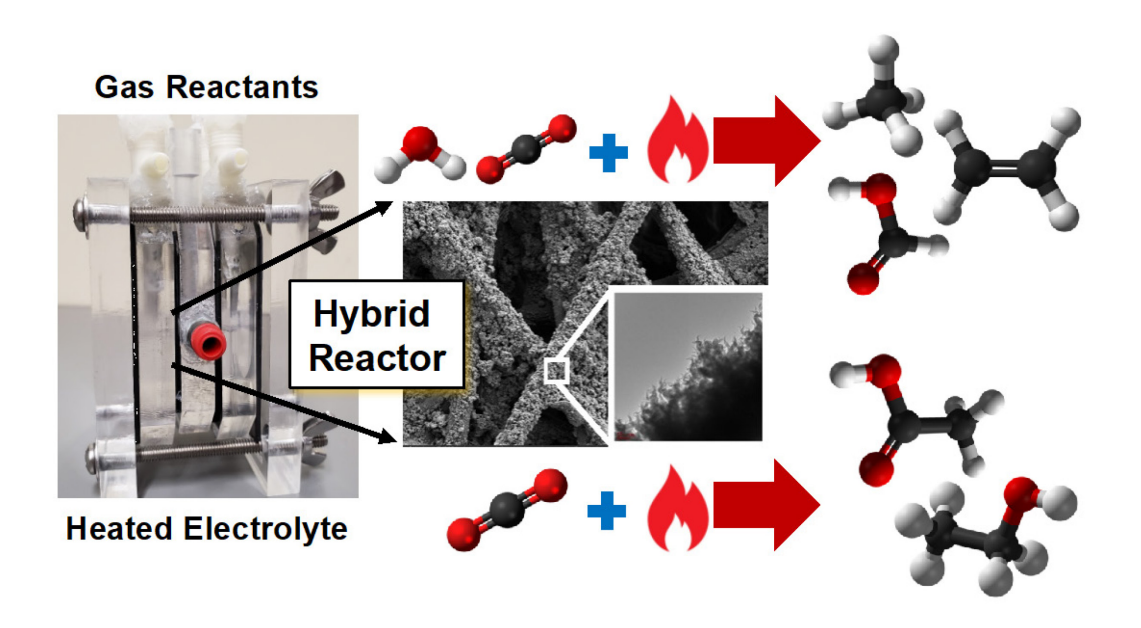
*Correspondence: heveritt@duke.edu; j.liu@duke.edu

Abstract

For the conversion of CO₂ into fuels and chemical feedstocks, hybrid gas/liquid-fed electrochemical flow reactors provide advantages in selectivity and production rates over traditional liquid phase reactors. However, fundamental questions remain about how to optimize conditions to produce desired products. Using an alkaline electrolyte to suppress hydrogen formation and a gas diffusion electrode catalyst composed of copper nanoparticles on carbon nanospikes, we investigate how hydrocarbon product selectivity in the CO₂ reduction reaction in hybrid reactors depends on three experimentally controllable parameters: (1) supply of dry or humidified CO₂ gas, (2) applied potential, and (3) electrolyte temperature. Changing from dry to humidified CO₂ dramatically alters product selectivity from C₂ products ethanol and acetic acid to ethylene and C₁ products formic acid and methane. Water vapor evidently influences product selectivity of reactions that occur on the gas-facing side of the catalyst by adding a source of protons that alters reaction pathways and intermediates.

Keywords: electrochemical flow reactor, CO₂ reduction reaction, hybrid gas/liquid reactor, product selectivity, three-phase interface

TOC Figure



In a hybrid gas phase/liquid phase reactor, C_1/C_2 product selectivity can be determined by externally controlled conditions: humidity, voltage, and temperature.

Introduction

Electrochemical conversion of carbon dioxide into fuel and chemical feedstocks offers a convenient way to turn carbon-containing compounds responsible for global climate change into valuable products such as methane, ethylene, and ethanol. Although traditional H-cells have been widely tested and characterized, they are not yet commercially viable due to the low solubility and long diffusion length of CO₂ in aqueous systems and associated mass transport limitations. Hybrid gas/liquid reactors have been developed as an alternative to overcome this mass transport limitation. The catalyst in hybrid gas/liquid reactors is deposited on one side of a gas-diffusion electrode (GDE), whose hydrophobic coating prevents the liquid electrolyte from leaking into the gas side. As a result, CO₂ gas flows through the gas-facing side of the GDE, and the reaction occurs at the three-phase gas-catalyst-liquid boundary. Studies of hybrid gas/liquid reactors have already demonstrated high current densities and high C₂ product selectivity (e.g. faradaic efficiency of C₂ ~ 85.8%), motivating growing interest in hybrid gas/liquid reactors for the CO₂ reduction reaction (CO2RR).

Despite these advantages, many questions remain about the performance of these hybrid reactors. For example, the CO2RR exhibits extreme sensitivity to changes in the local environment (pH, CO2 flow rate, water vapor concentration) at the three-phase boundary. ^{12,13} An alkaline electrolyte with high pH can be used to suppress the competing hydrogen evolution reaction (HER), ¹⁴ and the CO2RR rate is found to be proportional to CO2 flow rate. ¹⁵ Humidified CO2 can increase the stability of the GDE by preventing salt precipitation, ¹⁶ and moderate water concentration at GDE can facilitate hydrocarbon formation. ¹⁷ However, excess water at the cathode can inhibit CO2 gas diffusion to the catalyst at the three-phase boundary, ¹⁷ and a fast CO2 flow rate can suppress C2 product formation. ¹⁸ The extreme sensitivity of product distributions to local conditions at the gas-side suggest that the thermodynamics and kinetics of the CO2RR in the hybrid gas/liquid reactor are fundamentally different to those in

an H-cell.19

In particular, the exact role of water as a source of protons at the GDE remains unresolved in hybrid gas/liquid reactors. ^{19,20} Most of the desired CO2RR products are highly hydrogenated, and the CO2RR occurs with a sequential proton-coupled electron transfer (PCET) process. Protons must be available near the active intermediates of CO2RR to promote protonation and produce more hydrocarbons. ¹² However, protons can also be used to produce hydrogen through the competing HER. ²¹ To understand the role of water and its ability to supply protons, control of water concentration may be accomplished by adjusting the degree of GDE hydrophobicity. Thus, water management by adjusting the GDE hydrophobicity, adding water vapor to the CO₂ gas supply, and functionalizing catalytic surfaces for better water activation, has emerged as a critical need for optimizing product selectivity in hybrid gas/liquid reactors. ^{17,22} To date, very little work has been reported on how water delivery to the cathode influences CO2RR performance in any hybrid reactor architecture.

Electrolyte temperature and applied potential can also alter product selectivity. The electrolyte temperature changes the local and bulk pH, the concentration of dissolved CO₂, and the rate of diffusion of reactants to the electrode surface, all of which can affect hydrocarbon production.^{23,24} By contrast, the applied potential is known to change the binding energy of key intermediates on the catalyst surface and the reaction barrier of critical elementary steps.^{25,26} Increasing the applied potential usually decreases the reaction barriers for both hydrocarbon intermediates and hydrogen. In hybrid reactors, a given GDE catalyst requires a unique applied potential that maximizes the distribution of desired products and minimizes undesired products. All these parameters – proton supply, temperature, applied potential – affect product distributions, but these have not yet been investigated simultaneously to understand how product selectivity could be optimized in a hybrid gas/liquid reactor.

Here we report just such an investigation, finding that the addition of water vapor in the CO₂

supply to the gas-side of a hybrid gas/liquid reactor has a much greater effect on product selectivity than applied potential, while electrolyte heating increases the production of hydrogen and changes the relative selectivity of hydrocarbons, depending on the other conditions. Using a basic electrolyte (1M KOH) to suppress proton generation and HER,²¹ we investigated a CO2RR-supporting GDE catalyst composed of copper nanoparticles on carbon nanospikes (CNSs) on carbon fibers coated with hydrophobic polytetrafluoroethylene (PTFE) to minimize water diffusion to the catalyst. Under proton-limited conditions, we compared product distribution from both dry and humidified CO₂ gas supplies, observing that product distribution is dramatically changed by water vapor supply: formic acid and ethylene are enhanced while ethanol disappears and hydrogen is suppressed with humidified CO₂. These observations, some of which have been reported earlier,²⁷ are addressed in this expanded investigation that proposes reaction pathways to capture how product selectivity can be affected and controlled by external conditions. In addition to producing more hydrogen, higher electrolyte temperatures produced more formic acid and ethylene under humidified CO₂ conditions, while C₁ products were much less sensitive to temperature than C₂ products under dry CO₂ conditions. Higher applied potentials produced more hydrogen, but their effects on hydrocarbon products depended sensitively on humidification and temperature, as will be detailed below.

Experimental details

We used a standard three-electrode configuration – gas chamber, reference cell, and anodic cell – for the electrochemical CO2RR (Fig. 1).³ In our hybrid reactor, the CO2RR occurs at the three-phase (gas-catalyst-electrolyte) boundary of the gas-facing side of the cathode,^{4,5} while the oxygen evolution reaction (OER) occurs at the Pt mesh anode (Fig. 1B).¹ The CO₂ gas and water vapor flowed through the gas chamber, from which the liquid electrolyte in the

reference cell is separated by the GDE catalyst. 1M KOH was used as the electrolyte to limit proton availability from the electrolyte and suppress the HER.²¹ Although CO₂ was bubbled through the electrolyte, it remained strongly basic (see SI). All voltages are measured relative to a reversible hydrogen electrode (RHE). To control the electrolyte temperature, the reactor was placed in a water bath on a hot plate. The electrolyte temperature was measured by an epoxy-coated thermocouple attached to the catalyst in the reference cell and monitored by a temperature data logger (Fig. S1-2).

The GDE cathode used here was composed of randomly oriented carbon fibers (Fig. 1A) covered by a dense nanotextured array of CNSs approximately 50–80 nm in length. Each nanospike consisted of layers of puckered carbon, ending in a ~2 nm wide curled tip (Fig. S3). Copper nanoparticles (NPs) were used since they are widely used as effective hydrocarbon catalysts. A catalyst ink was produced with copper NPs (0.1 g), methanol, nafion, and 0.01 g of PTFE particles, and the distribution of copper can be controlled by adjusting the ratio of copper NPs in the ink. The ink was spray-cast onto the CNS cathode, producing a copper NP density of ~55 mg/cm². To minimize electrolyte contact with the catalyst so that it could be wetted without leaking and allowing the CO2RR to occur at the three-phase boundary, the carbon fibers were coated by a hydrophobic layer of PTFE. Although this approach reduced total current density, it increased the current stability and prevented electrolyte leaking during the experiment (Fig. S4).

The catalyst facing the electrolyte is fully wetted, and the catalyst facing the gas chamber is dry or partially wetted due to the hydrophobic coating of PTFE on the GDE (Fig. 1).^{4,5} The CO2RR occurs at the three-phase boundary, where liquid products (formic acid, ethanol, acetic acid) are drawn toward the fully wetted catalyst facing the electrolyte and are measured later by NMR, while gas products (hydrogen, methane, ethylene) leave the drier catalyst facing the gas chamber and are measured in real time by a quadrupole mass

spectrometer. Details about the quantitative measurements of concentrations, Faraday efficiencies, current stability, and production rates are provided in the SI.

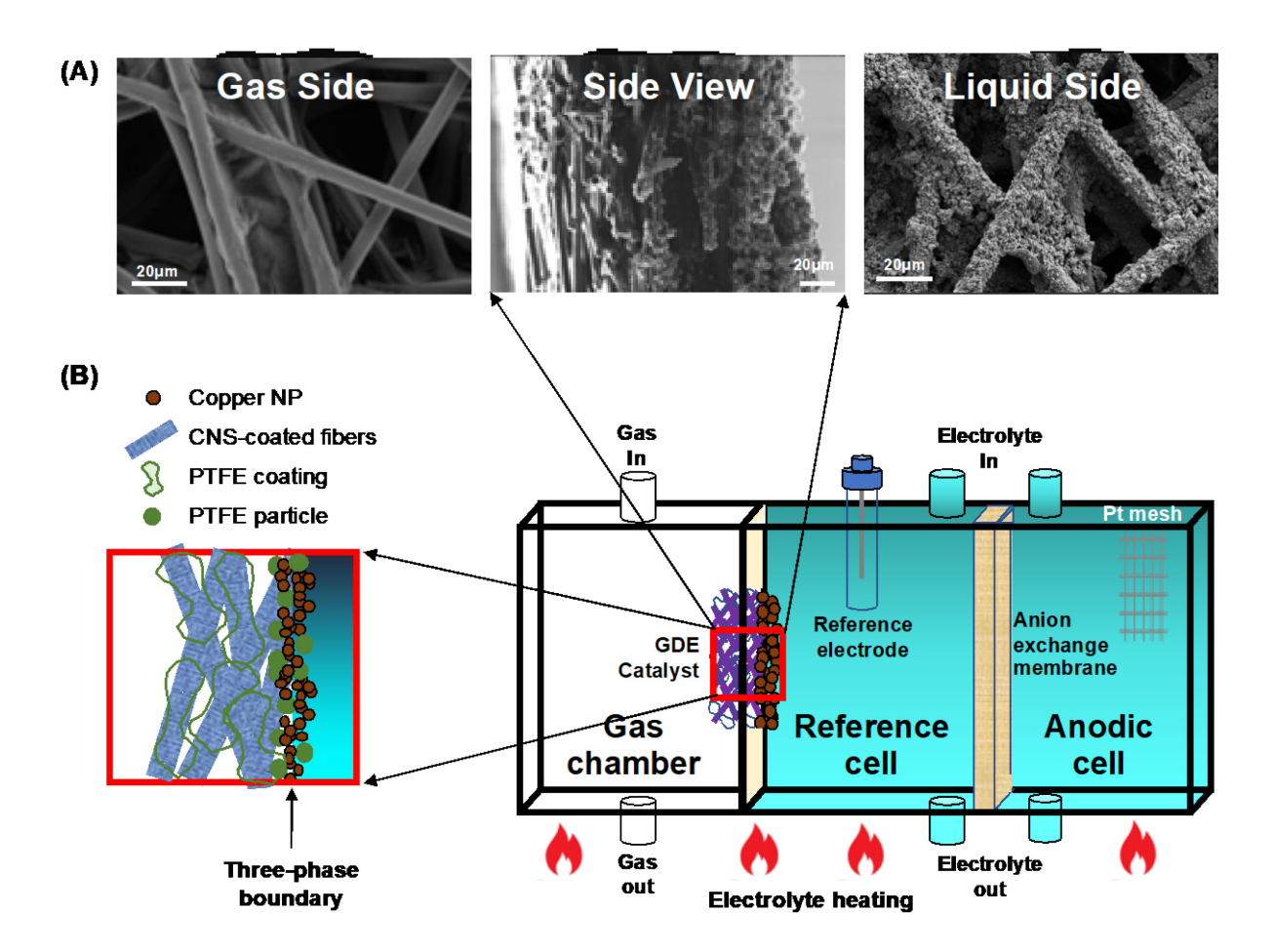


Fig. 1. (A) Scanning electron microscope images of the CNS-coated GDE catalyst, showing the carbon fibers (gas-side) coated with copper NPs (liquid-side) from which the CNSs extend. The nonconductive PTFE is not observable in these SEM images. The center shows a side view of the entire GDE catalyst. (B) Illustration of the three-cell hybrid gas/liquid reactor (a prototype RW-HV1.2 by Reactwell), with the GDE separating the gas and reference cells and the anion exchange membrane separating the reference and anodic cells. The expanded illustration of the GDE shows the three-phase boundary.

Results and discussion

1. Dry and humidified CO₂ conditions at room temperature.

In order to understand the role of water vapor in the hybrid gas/liquid reactor for the CO2RR, we begin with a control experiment to compare products formed by supplying dry CO₂ ("CO₂") or humidified CO₂ ("CO₂ + H₂O") in the gas chamber at room temperature (23.5°C). Dry CO₂ gas flowed through the gas chamber at a rate of 10 ml/min. Water vapor was added by bubbling dry CO₂ through a small water bottle for an hour before being diverted into the gas chamber, after which the supply became 2.7% water vapor and 97.3% CO₂. All other conditions remain unchanged for all experiments, including the electrolyte (CO₂-dissolved 1M KOH), so the effects of gas-side conditions on product selectivity may be revealed.

The total current density at -0.8V vs. RHE slightly increased when humidified CO₂ replaced dry CO₂ (Fig. 2A, B, D, and F). Even though the highly alkaline electrolyte KOH was used to suppress HER, hydrogen remained the principal product, with a production rate of ~50 nmole/s·cm² for both dry and humidified CO₂. The total hydrocarbon production rate increased with humidification by about two times ($\sim 6.3 \rightarrow 13$ nmole/s·cm²). Moreover, dry CO₂ produced comparable amounts of C₁ and C₂ products (~ 3 nmole/s·cm² each), but humidified CO₂ favored C₁ products over C₂ products by 4:1.²⁷

Regarding C_2 products, both dry and humidified CO_2 favor ethylene production. Dry CO_2 produced comparable amounts of acetic acid and ethanol (~ 0.5 nmole/s·cm² each), while humidified CO_2 enhanced ethylene production while suppressing acetic acid and eliminating ethanol entirely. For C_1 products, methane was unaffected by the introduction of water vapor, but formic acid was enhanced more than four times. Thus, humidification favors formic acid and ethylene while hindering acetic acid and eliminating ethanol without significantly affecting hydrogen or methane under these control conditions.

At a larger applied potential (-1.0V vs. RHE), the total current density increased by the same amount under both dry and humidified CO₂ conditions (Fig. 2A). Although hydrogen

production increased compared to -0.8 V for both conditions, it didn't increase as much under humidified CO₂ (~69 nmole/s·cm²) compared to dry CO₂ (~89 nmole/s·cm²) (Fig. 2C, E, and G). Total hydrocarbon production only slightly decreased compared to the -0.8 V case, and humidification again increased the total hydrocarbon production rate by about two times.

As before, dry CO₂ produced comparable amounts of C₁ and C₂ products (~ 3 nmole/s·cm² each), but humidified CO₂ favored C₁ products over C₂ products even more, by 5:1. However, the distribution of C₂ products changed significantly, with acetic acid replacing suppressed ethylene as the dominant C₂ product under dry conditions, but ethylene returned as the dominant C₂ product under humidification. As before, humidified CO₂ eliminated ethanol production, and it even more dramatically suppressed acetic acid. As for C₁ products, the higher applied voltage significantly suppressed methane production under dry conditions, while formic acid remained the dominant hydrocarbon product, especially under humidified conditions, with rates comparable to the -0.8V case. So carboxylic acids (O₂ products) are the dominant hydrocarbons formed at -1.0V: comparable formic acid and acetic acid for dry CO₂, and copious formic acid for humidified CO₂.

Summarizing these control experiments at room temperature, hydrogen is the dominant product for both dry and humidified CO₂, increasing with increasing bias. Total hydrocarbon production increased with humidification but was relatively insensitive to bias. For both applied potentials, humidified CO₂ suppressed C₂ products except for ethylene while enhancing C₁ products, especially formic acid. Acetic acid and ethanol strongly favor dry CO₂ conditions. These results show that increasing the applied potential and especially the addition of water vapor to the gas chamber have a significant effect on product selectivity.

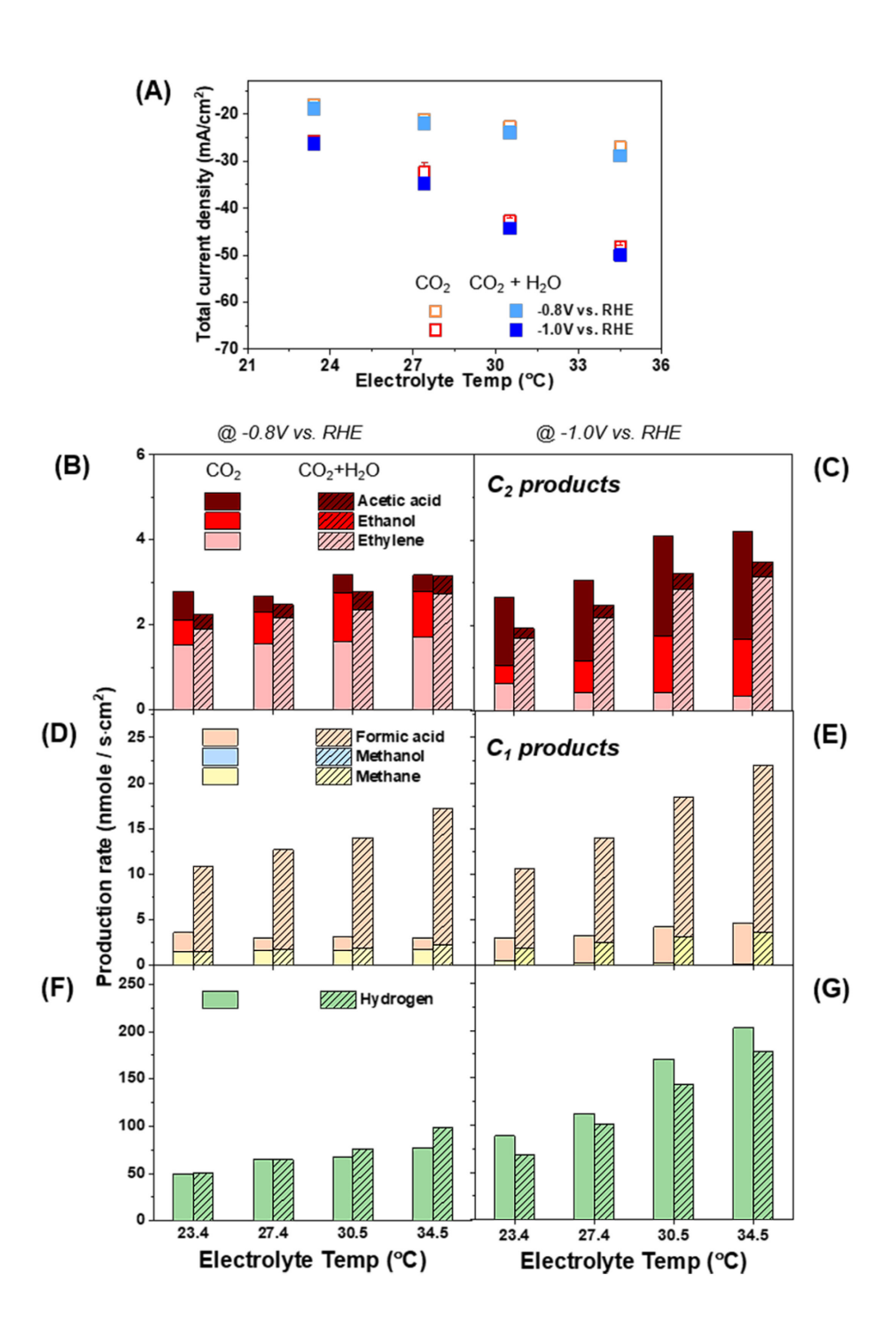


Fig. 2. (A) Total current density at -0.8V and -1.0V vs RHE at different electrolyte temperatures under the dry and humidified CO₂ conditions. Hollow boxes are for dry CO₂ conditions and solid boxes are for humidified CO₂ conditions. Production rate of C₂ (B, C), C₁ (D, E), and hydrogen (F, G) at different electrolyte temperatures and potentials under the dry CO₂ (solid boxes) and humidified CO₂ (hashed boxes) conditions.

2. Effect of electrolyte temperature.

Guided by the room temperature control experiments, we next explored how product selectivity changed with increasing electrolyte temperature. As expected, total current density increased with increasing temperature: for both dry and humidified CO₂ conditions at 34.5°C the current density increased by ~50% at -0.8V and ~90% at -1.0V. Production rates for almost all products increased with increasing temperature, but how they increased depended sensitively on other conditions. Most strongly affected by increasing temperature was the production rate of hydrogen, which more than doubled from room temperature to 34.5°C under all conditions. Interestingly, hydrogen production preferred humidified CO₂ at -0.8V but dry CO₂ at -1.0V.

Using dry CO₂, the ethanol production rate increased most significantly with temperature, by up to ~200% at 34.5°C at -1.0V, a larger percentage than the total current density increased. The production rates for the other hydrocarbon products remained fairly constant at -0.8V, except for formic acid which actually decreased with increasing temperature. By contrast, hydrocarbon products exhibited greater temperature sensitivity with dry CO₂ at -1.0V, with formic acid, acetic acid, and ethanol production rates increasing but methane and ethylene decreasing with increasing temperature.

By contrast, for humidified CO_2 the hydrocarbon product selectivity exhibited nearly identical temperature dependence for either applied potential. Formic acid and ethylene production rates grew significantly (by $\sim 112\%$ and 84%, respectively, at -1.0V), while methane and acetic acid remained relatively insensitive to temperature.

In summary, increasing temperature generally increased production rates, especially for hydrogen, but hydrocarbon product selectivity depended more on gas conditions and applied potential, whose effects were amplified with increasing temperature. How these findings may be understood in the context of this GDE catalyst in this hybrid reactor will be

explored next.

3. Product selectivity.

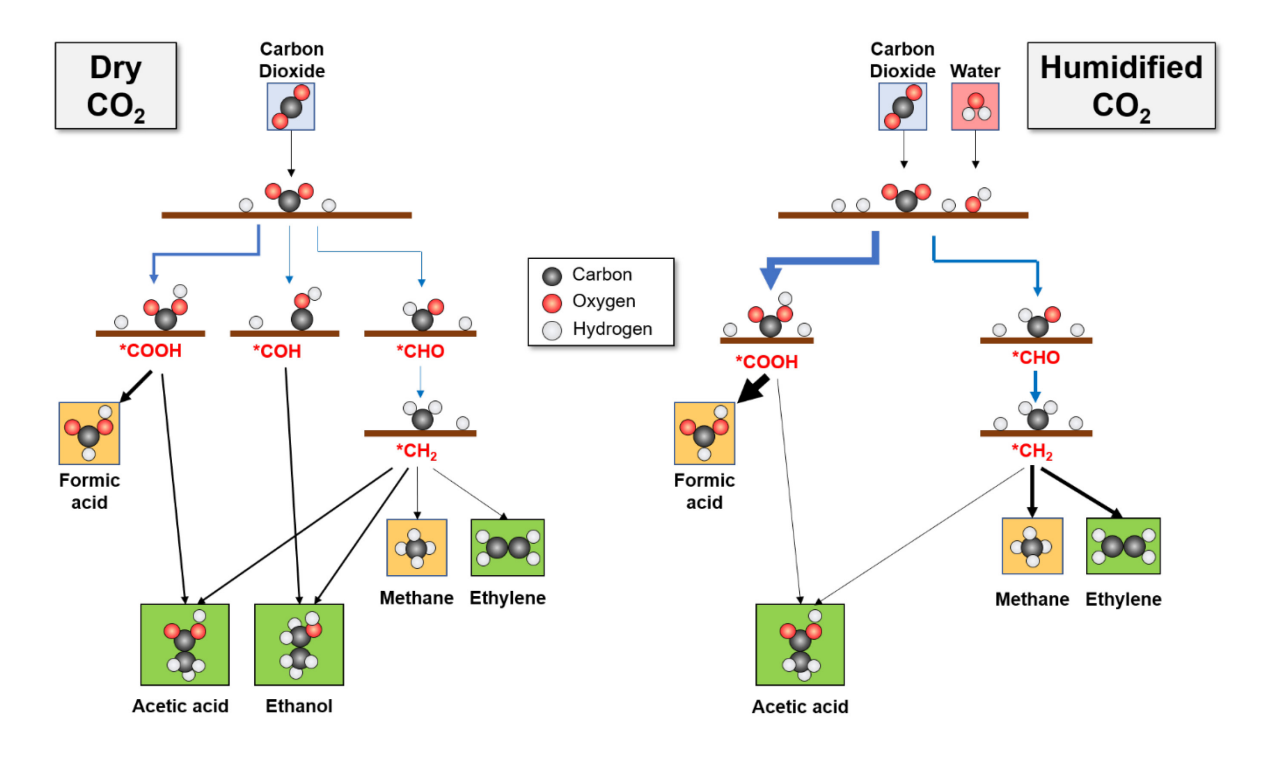
Hydrogen is the dominant product under all conditions, regardless whether Ar (prior work²⁷) or dry CO₂ is supplied in the gas chamber. When only Ar was supplied to the gas chamber, hydrogen was by far the dominant product (faradaic efficiency > 90%, compared to <1% hydrocarbon). Consequently, the HER must be active on the liquid-facing side of the GDE catalyst, and hydrogen must diffuse through to the gas chamber to be detected. This also indicates that protons from the aqueous electrolyte diffuse toward and adsorb onto the gas-facing side of the catalyst, then react with adsorbed CO₂ to produce hydrocarbon products.^{3,29} The changes in hydrogen and hydrocarbon production following introduction of humidified CO₂ suggest that water vapor further affects the availability of protons on the side of the catalyst facing the gas chamber. Indeed, hydrocarbon production is very sensitive to the presence or absence of water vapor in the CO₂ gas feed, confirming that hydrocarbons are produced on the gas-facing side of the GDE catalyst.

We may conclude that the surface of the catalyst facing the liquid side is covered by hydrogen, while the gas-facing surface contains varying amounts of hydrogen and critical hydrogenated hydrocarbon intermediates. It has been reported that the enhanced hydrogen formation enhances electrocatalytic CO2RR to produce formate, ^{10,30} ethylene, ¹⁰ and alcohol products (esp. ethanol), ³¹ instead of HER. Hydrocarbon intermediates in our hybrid reactor also include carboxylic acid radicals *COOH formed by hydrogenating adsorbed CO₂ to produce formic acid and acetic acid. Dissociative adsorption of CO₂ and subsequent hydrogenation of the CO intermediate toward either *COH or *CHO produce additional essential intermediates, as will be discussed below.^{32,33}

In our experiments, methanol and **carbon monoxide** are not produced. This indicates that O_1 products other than water are inhibited in favor of O_0 alkanes and alkenes and O_2

carboxylic acids. We surmise that instead of desorbing, dissociatively adsorbed *CO quickly binds hydrogen to form critical intermediates *COH or *CHO that produce all the hydrocarbon products except the carboxylic acids (produced by *COOH).

C₁ or C₂ products were favored depending on whether the CO₂ in the gas chamber was humidified or dry, respectively. Dry CO₂ produced comparable amounts of the O₀ hydrocarbons methane and ethylene and comparable amounts of the O₂ hydrocarbons formic acid and carboxylic acid, indicating a catalytic environment favorable for C₂ product formation. Humidified CO₂ also produced comparable amounts of the O₀ hydrocarbons methane and ethylene, more than with dry CO₂, but dramatically enhanced the O₂ hydrocarbon formic acid while suppressing acetic acid. The O₁ hydrocarbon ethanol was only created under dry CO₂ conditions. These observations indicate that as compared to dry CO₂, humidified CO₂ favors C₁/O₀, C₂/O₀, and especially C₁/O₂ products but suppresses C₂/O₂ products and prevents all O₁ hydrocarbons. The mechanisms responsible for this selectivity are discussed next and summarized in Scheme 1.



Scheme 1. Possible C_1 and C_2 reaction pathways under dry and humidified CO_2 conditions.

The arrows indicate whether proton, electron, or proton-coupled electron transfers take place, and the width of the arrows indicates propensity. Orange boxes are C₁ products, and green boxes are C₂ products.

Formic acid is the principal hydrocarbon produced under all conditions, except for dry CO₂ at elevated temperatures. As illustrated in Scheme 1, formic acid is easily produced following the hydrogenation of adsorbed CO₂ from two adsorbed protons and two electrons. Humidified CO₂ produced much more formic acid, more in fact than all the other hydrocarbons combined. To understand why water vapor so dramatically enhanced formic acid production, consider that acetic acid production exhibits an interesting correlation/anti-correlation relationship with formic acid: under dry CO₂ conditions both production rates increase or decrease in a similar manner with applied potential and temperature, while under humidified CO₂ conditions, formic acid production rates skyrocket while acetic acid production is suppressed.

Although there is some debate about key intermediates in CO2RR,¹² the common intermediate for both formic and acetic acid is the carboxylic acid radical *COOH, which is easily formed under either dry or humidified CO₂ conditions after proton transfer from CO₂⁻ or directly from CO₂ activation. Acetic acid likely forms when *COOH interacts with the reduced *CH₃ species adsorbed on the catalytic surface.³⁴ (An alternative mechanism has been proposed in which *CH₂ binds to *CO to produce *CO-CH₂.³⁵ Since *CO tends to bind *CH₂ rather than to desorb, this may also explain why CO wasn't detected.)

So the addition of water vapor in the gas chamber must somehow inhibit C-C bond formation in favor of additional hydrogenation of the intermediate. It is known that formic acid can share with hydrogen a common intermediate anionic hydride (H⁻), ¹² so increasing hydrogen adsorption on the catalyst also produces more formic acid. Conversely, C-C bond formation

appears to be inhibited by an abundance of adsorbed protons. So under dry CO₂ conditions, the dearth of adsorbed protons on the gas-facing side of the catalyst allowed C-C bonds sufficient time and electrons to form. The addition of water vapor supplied additional protons that hydrogenated the intermediate and produced formic acid before C-C bonds could form.

Methane is the other C_1 product produced in measurable quantities, but its dependence on conditions differs from what is observed for formic acid, indicating a different pathway with different intermediates. It is instructive to compare methane production to the other observed O_0 product **ethylene**, noting that no other C_2/O_0 hydrocarbons are detected (i.e. **ethane** and **acetylene**). Both methane and ethylene, which contain four protons and respectively require eight and twelve electrons, not only exhibit the same dependence on gas conditions, voltage, and temperature, both are produced in nearly equal amounts in each case (Fig. S5). Both prefer humidified CO_2 , higher voltage, and higher temperatures, and both are suppressed with dry CO_2 under the same higher potential and temperatures. This suggests they share similar reaction pathways with common intermediates.

To produce methane (and C_2 products), adsorbed intermediates *COOH and *CO must be further reduced to *COH and/or *CHO intermediates, requiring a supply of protons. The observation that humidified CO_2 produced more methane and ethylene than dry CO_2 further supports the hypothesis that the gas side-facing catalyst is starved of adsorbed protons under dry CO_2 . The additional protons supplied by humidified CO_2 favor the *CHO \rightarrow *CH2 intermediates that form the hydrogenated hydrocarbons methane and ethylene (see Scheme 1). It has been proposed that methane formation follows the protonation processes *COOH \rightarrow *CO \rightarrow *CHO \rightarrow CH₄. ³⁶ For ethylene formation, a hydrogen-assisted C-C coupling mechanism has been suggested for a fluorine-modified copper catalyst that enhanced water dissociation to produce more *H and promote the hydrogenation of *CO to *CHO. ¹⁰ The subsequent hydrogen-assisted C-C coupling of *CHO \rightarrow *OHCCHO was energetically more

favorable than the dimerization of *CO \rightarrow CO-CO.

The mechanisms that benefit from humidified CO_2 come at the expense of C_2/O_1 ethanol and C_2/O_2 acetic acid production. Although the *CHO intermediate is favored by humidified CO_2 , the *COH intermediate is needed to produce ethanol, just as the *COOH intermediate is needed to produce acetic acid. We have just seen that when humidified CO_2 adds a significant number of protons to the gas-facing side of the catalyst, hydrogen binds to *COOH to produce formic acid and substitutes for oxygen in *CHO \rightarrow *CH₂ to produce methane and ethylene. Ethanol is not produced under these conditions. By contrast, both *COH and *CHO coexist under dry CO_2 conditions due to the dearth of protons, and ethanol is produced (see Scheme 1).

Another explanation for the suppressed production of ethanol (and acetic acid) with humidified CO₂ is that these C₂ products share a common intermediate: *CO-CHO or *CO-COH. 32,37,38 If true, one of the C₂ products increases at the expense of the other C₂ products, just as we observed: humidified conditions favor ethylene, while dry conditions favor ethanol and acetic acid, especially at -1.0V vs. RHE. Ethanol formation is known to have a greater reduction potential at -0.744 V vs. RHE than acetic acid and ethylene.³⁹ Thus, when ethylene formation is enhanced, the other C₂ products (acetic acid and ethanol) are suppressed, and vice versa.

Methanol was not observed under any conditions, perhaps a surprising result since ethanol is produced, albeit with dry CO₂. All the previous results indicate that when copious protons are available, hydrogen aggressively substitutes for oxygen in key intermediates. The carboxylic acids are formed either by a single hydrogenation step (formic acid) or by binding *COOH to a fully formed *CH₃ radical (needed for acetic acid). To produce methanol, the *COH radical must be fully hydrogenated, which apparently doesn't happen without sacrificing the hydroxyl to produce methane. Like acetic acid, ethanol must therefore be formed

by combining two intermediates: *COH and *CH₃. It has already been shown that the reduction of *CH₃O to methane has a lower energy barrier than to methanol, ^{32,39} confirming why methane formation was favored over methanol. Methanol may even compete with ethylene, whose the reduction potential is lower than methanol even though C-C coupling is required. ⁴⁰

4. Effects of electrolyte heating and applied potential

In every case, increasing electrolyte temperature either increased or perhaps decreased, production rates but only indirectly affected product selectivity. As noted above, hydrogen production was most accelerated by elevated temperatures, while production of select hydrocarbons also grew, depending on the other conditions. It has been reported that heating reduces the concentration of CO₂ gas dissolved in the electrolyte solution, allowing the competing HER to increase while suppressing hydrocarbon formation.^{23,41} This helps explain the enhanced hydrogen formation with increasing the electrolyte temperature under both dry CO₂ and humidified CO₂ conditions.

The increase in hydrogen, formic acid, and ethylene production under heated humidified conditions indicates that not only is hydrogen gas increasingly desorbing but that protons are increasingly diffusing through the GDE catalyst in order to hydrogenate hydrocarbon intermediates. A similar trend is seen under dry conditions, except that in this case the hydrogenation process is slower, allowing greater opportunities for C-C bond formation through the binding of separately hydrogenated or pristine intermediates. Thus, temperature affects product selectivity primarily by how it affects the supply of protons.

By contrast, increasing applied potential did change hydrocarbon selectivity, but only under dry CO₂ conditions where higher voltage significantly favors formic acid, ethanol, and acetic acid while suppressing methane and ethylene. Under humidified conditions, increasing voltage just increased production rates without significantly affecting selectivity. Except for hydrogen and formic acid, which require 2 electrons to form a molecule, all observed

hydrocarbon products require 8 or 12 electrons to form a molecule. For both CO₂ conditions, the current nearly doubles when applied potential increases from -0.8V to -1.0V. At the same time, the production rates of hydrogen, formic acid, and acetic acid more than double with dry CO₂. Since production rates depend on measured current, the commensurate increase in production of these products reveals that their Faraday efficiency is not affected by potential. However, the production rates for methane and ethylene are cut by more than a factor of two, suggesting that their Faraday efficiencies drop by more than four times, from $6.1 \rightarrow 0.8\%$ and from $8.9 \rightarrow 1.7\%$ from -0.8V to -1.0V, respectively (Fig. S6). This may indicate that another factor in selectivity under dry CO₂ conditions is the availability of electrons for these products, which are already struggling because of the absence of adsorbed protons.

Conclusion

In summary, CO2RR in a hybrid gas/liquid reactor was investigated to ascertain how hydrocarbon product selectivity depended on reactor conditions. To suppress hydrogen formation, we used a basic electrolyte and a PTFE hydrophobic coating on the carbon nanospike/copper nanoparticle catalyst. We controlled three parameters in this hybrid reactor: (1) dry or humidified CO₂ reactants in the gas chamber, (2) electrolyte temperature (23.5 to 34.5°C), and (3) applied potential (-0.8V or -1.0V vs. RHE). Because of the hydrophobic layer, the catalyst facing the gas chamber is only partially wetted. Consequently, the catalyst facing the gas chamber is starved of protons, and we wanted to explore how water vapor provided through the gas chamber supplies hydrogen and changes reaction pathways, intermediates, and products.

We find that product selectivity was dramatically changed when dry CO₂ was humidified with water vapor, while temperature did not affect product selectivity and applied potential only affected selectivity for dry CO₂. Specifically, humidified CO₂ produced more

hydrogen that, in turn, helped produce more C₁ products while suppressing the C-C bonding needed for C₂ products. More products are produced with increasing temperature, especially hydrogen, which indirectly affected hydrocarbon selectivity. Humidified CO₂ produced more C₁ (formic acid and methane) and ethylene with increasing the temperature, suggesting that those products are starved for hydrogen (or methyl groups) and the water vapor provides it. Because of the strong hydrophobic environments of the GDE catalyst, dry CO₂ starves the surface of hydrogen, explaining why methane and ethylene decrease with temperature since they are starved for hydrogen and receive none from the gas side. However, this dearth of protons yields greater C₂ production by allowing C-C bonds time to form. Because carboxylic acid *COOH and *COH radicals are preserved in this environment, formic acid, acetic acid, and ethanol dominate.

Our results indicate that managing water vapor content in the supply of gaseous CO₂ in a hybrid reactor is a key parameter for beneficially controlling CO2RR product selectivity. Moreover, by elevating the electrolyte temperature both current and production rate increase, thereby overcoming a key obstacle historically hindering adoption of hybrid gas/liquid reactors.

Author contributions

S.-H.L. built the experimental setup, synthesized and characterized the catalyst, and performed all of the measurements. B.I. built the hybrid gas/liquid reactor. All of the authors analyzed data, contributed to writing the manuscript, and have given approval to the final version of the manuscript

Conflicts of interest

There are no conflicts to declare

Acknowledgments

The authors acknowledge the early help and supply of the CNS from Yang Song and Dale Hensley. This research was supported in part by the National Science Foundation (grant number CHE-1954838). The authors also acknowledge support by the Duke University Shared Materials Instrumentation Facility (SMIF), a member of the North Carolina Research Triangle Nanotechnology Network (RTNN), which is supported by the National Science Foundation (Grant ECCS-1542015) as part of the National Nanotechnology Coordinated Infrastructure (NNCI). This research was supported in part by an appointment of S.-H. L. to the Department of Defense (DOD) Research Participation Program administered by the Oak Ridge Institute for Science and Education (ORISE) through an interagency agreement between the U.S. Department of Energy (DOE) and the DOD. ORISE is managed by ORAU under DOE contract number DE-SC0014664. All opinions expressed in this paper are the author's and do not necessarily reflect the policies and views of DOD, DOE, or ORAU/ORISE.

References

- 1 M. B. Ross, P. De Luna, Y. Li, C.-T. Dinh, D. Kim, P. Yang and E. H. Sargent, *Nat. Catal.*, 2019, **2**, 648-658.
- 2 P. D. Luna, C. Hahn, D. Higgins, S. A. Jaffer, T. F. Jaramillo and E. H. Sargent, *Science*, 2019, **364**, eaav3506.
- 3 K. Liu, W. A. Smith and T. Burdyny, ACS Energy Lett., 2019, 4, 639-643.
- 4 M. Jouny, W. Luc and F. Jiao, Nat. Catal., 2018, 1, 748-755.
- 5 L.-C. Weng, A. T. Bell and A. Z. Weber, *Phys. Chem. Chem. Phys.*, 2018, **20**, 16973-16984.
- 6 M. Alfath and C. W. Lee, Catalysts, 2020, 10, 859.
- 7 D. Higgins, C. Hahn, C. Xiang, T. F. Jaramillo and A. Z. Weber, ACS Energy Lett., 2019, 4, 317-324.
- 8 C.-T. Dinh, T. Burdyny, M. G. Kibria, A. Seifitokaldani, C. M. Gabardo, F. P. G. d. Arquer, A. Kiani, J. P. Edwards, P. D. Luna, O. S. Bushuyev, C. Zou, R. Quintero-Bermudez, Y. Pang, D. Sinton and E. H. Sargent, *Science*, 2018, **360**, 783-787.

- 9 F. P. G. d. Arquer, C.-T. Dinh, A. Ozden, J. Wicks, C. McCallum, A. R. Kirmani, D.-H. Nam, C. Gabardo, A. Seifitokaldani, X. Wang, Y. C. Li, F. Li, J. Edwards, L. J. Richter, S. J. Thorpe, D. Sinton and E. H. Sargent, *Science*, 2020, 367, 661-666.
- 10 W. Ma, S. Xie, T. Liu, Q. Fan, J. Ye, F. Sun, Z. Jiang, Q. Zhang, J. Cheng and Y. Wang, *Nat. Catal.*, 2020, **3**, 478-487.
- 11 T. N. Nguyen and C.-T. Dinh, Chem. Soc. Rev., 2020, 49, 7488-7504.
- 12 Y. Y. Birdja, E. Pérez-Gallent, M. C. Figueiredo, A. J. Göttle, F. Calle-Vallejo and M. T. M. Koper, *Nat. Energy*, 2019, **4**, 732-745.
- 13 D. Gao, R. M. Arán-Ais, H. S. Jeon and B. Roldan Cuenya, Nat. Catal., 2019, 2, 198-210.
- 14 S. Verma, X. Lu, S. Ma, R. I. Masel and P. J. A. Kenis, *Phys. Chem. Chem. Phys.*, 2016, **18**, 7075-7084.
- 15 R. Kas, K. K. Hummadi, R. Kortlever, P. de Wit, A. Milbrat, M. W. J. Luiten-Olieman, N. E. Benes, M. T. M. Koper and G. Mul, *Nat. Commun.*, 2016, 7, 10748.
- 16 M. E. Leonard, L. E. Clarke, A. Forner-Cuenca, S. M. Brown and F. R. Brushett, *ChemSusChem*, 2020, **13**, 400-411.
- 17 E. W. Lees, B. A. W. Mowbray, F. G. L. Parlane and C. P. Berlinguette, *Nat. Rev. Mater.*, 2022, 7, 55-64.
- 18 Y. C. Tan, K. B. Lee, H. Song and J. Oh, Joule, 2020, 4, 1104-1120.
- 19 D. M. Weekes, D. A. Salvatore, A. Reyes, A. Huang and C. P. Berlinguette, *Acc. Chem. Res.*, 2018, **51**, 910-918.
- 20 Q. Dong, X. Zhang, D. He, C. Lang and D. Wang, ACS Cent. Sci., 2019, 5, 1461-1467.
- 21 C.-T. Dinh, F. P. García de Arquer, D. Sinton and E. H. Sargent, ACS Energy Lett., 2018, 3, 2835-2840.
- 22 A. Reyes, R. P. Jansonius, B. A. W. Mowbray, Y. Cao, D. G. Wheeler, J. Chau, D. J. Dvorak and C. P. Berlinguette, ACS Energy Lett., 2020, 5, 1612-1618.
- 23 S. T. Ahn, I. Abu-Baker and G. T. R. Palmore, Catalysis Today, 2017, 288, 24-29.
- 24 A. Löwe, C. Rieg, T. Hierlemann, N. Salas, D. Kopljar, N. Wagner and E. Klemm, *ChemElectroChem*, 2019, **6**, 4497-4506.

- 25 J. Hussain, H. Jónsson and E. Skúlason, ACS Catal., 2018, **8**, 5240-5249.
- 26 S.-T. Gao, S.-Q. Xiang, J.-L. Shi, W. Zhang and L.-B. Zhao, *Phys. Chem. Chem. Phys.*, 2020, **22**, 9607-9615.
- 27 S.-H. Lee, Y. Song, B. Iglesias, H. O. Everitt and J. Liu, ACS Appl. Energy Mater., 2022, 5, 9309-9314.
- 28 Y. Song, R. Peng, D. K. Hensley, P. V. Bonnesen, L. Liang, Z. Wu, H. M. Meyer III, M. Chi, C. Ma, B. G. Sumpter and A. J. Rondinone, *ChemistrySelect*, 2016, 1, 6055-6061.
- 29 T. Burdyny and W. A. Smith, Energy Environ. Sci., 2019, 12, 1442-1453.
- 30 W. Ma, S. Xie, X.-G. Zhang, F. Sun, J. Kang, Z. Jiang, Q. Zhang, D.-Y. Wu and Y. Wang, *Nat. Commun.*, 2019, **10**, 892.
- 31 J. Li, A. Xu, F. Li, Z. Wang, C. Zou, C. M. Gabardo, Y. Wang, A. Ozden, Y. Xu, D.-H. Nam, Y. Lum, J. Wicks, B. Chen, Z. Wang, J. Chen, Y. Wen, T. Zhuang, M. Luo, X. Du, T.-K. Sham, B. Zhang, E. H. Sargent and D. Sinton, *Nat. Commun.*, 2020, 11, 3685.
- 32 W. Luo, X. Nie, M. J. Janik and A. Asthagiri, ACS Catal., 2016, 6, 219-229.
- 33 A. J. Garza, A. T. Bell and M. Head-Gordon, ACS Catal., 2018, 8, 1490-1499.
- 34 Z. Sun, T. Ma, H. Tao, Q. Fan and B. Han, Chem, 2017, 3, 560-587.
- 35 Y. Zheng, A. Vasileff, X. Zhou, Y. Jiao, M. Jaroniec and S.-Z. Qiao, *J. Am. Chem. Soc.*, 2019, **141**, 7646-7659.
- 36 X. Wang, A. Xu, F. Li, S.-F. Hung, D.-H. Nam, C. M. Gabardo, Z. Wang, Y. Xu, A. Ozden, A. S. Rasouli, A. H. Ip, D. Sinton and E. H. Sargent, J. Am. Chem. Soc., 2020, 142, 3525-3531.
- 37 W. Luc, X. Fu, J. Shi, J.-J. Lv, M. Jouny, B. H. Ko, Y. Xu, Q. Tu, X. Hu, J. Wu, Q. Yue, Y. Liu, F. Jiao and Y. Kang, *Nat. Catal.*, 2019, **2**, 423-430.
- 38 S. Hanselman, M. T. M. Koper and F. Calle-Vallejo, ACS Energy Lett., 2018, 3, 1062-1067.
- 39 L. Fan, C. Xia, F. Yang, J. Wang, H. Wang and Y. Lu, Sci. Adv., 2020, 6, eaay3111.
- 40 K. J. P. Schouten, Z. Qin, E. Pérez Gallent and M. T. M. Koper, *J. Am. Chem. Soc.*, 2012, **134**, 9864-9867.
- 41 P. Lobaccaro, M. R. Singh, E. L. Clark, Y. Kwon, A. T. Bell and J. W. Ager, *Phys. Chem. Chem. Phys.*, 2016, 18, 26777-26785.